

# New Views on Carrier Diffusion and Recombination by Combining Small Perturbation Techniques: Application to BiVO<sub>4</sub> Photoelectrodes

Agustin O. Alvarez,\* Miguel García-Tecedor, Laura Montañés, Elena Mas-Marzá, Sixto Giménez, and Francisco Fabregat-Santiago\*

Impedance spectroscopy (IS), intensity-modulated photocurrent spectroscopy (IMPS), and intensity-modulated photovoltage spectroscopy (IMVS) are well-established powerful modulated techniques to characterize optoelectronic devices. Their combined use has proven to provide an understanding of the behavior and performance of these systems, far beyond the output obtained from their independent analysis. However, this combination is shown to be challenging when applied to complex systems. Herein, IS, IMPS, and IMVS are cooperatively used, for the first time, to study the distributed photogeneration, diffusion, and recombination processes in a photoanode of zircon-doped bismuth vanadate. The use of this methodology reveals that the carriers that determine the response of the device are the electrons when the device is illuminated from the hole-collector side (electrolyte) and the holes when the illumination reaches the device from the electron-collector side. Detailed quantitative information is obtained for each carrier, including recombination lifetime, diffusion coefficient and collection and separation efficiencies, identifying the latter as the main limitation of this device. This methodology is a powerful tool that can be used for the characterization and understanding of the operating processes of other photoconversion devices.

standing as some of the main systems that will help to overcome the global dependence on fossil fuels. Photovoltaic devices are already generating electrical energy from sunlight massively in the world. The conversion of sunlight into fuels and chemicals is also an attractive and growing field,<sup>[1]</sup> mainly driven by the photoelectrochemical production of H<sub>2</sub> from the oxidation of H<sub>2</sub>O.<sup>[2]</sup>

During the operation of photoconversion devices, the overall performance is determined by several optoelectronic processes (carrier generation, transport, recombination, and charge transfer). Consequently, an appropriate characterization of these processes is essential for a reliable understanding of the operation mechanism. This knowledge makes it possible to identify the limitations of the system, thus favoring their optimization and even the development of new devices. Impedance spectroscopy (IS),<sup>[3–5]</sup> intensity-modulated photocurrent spectroscopy

(IMPS),<sup>[6–8]</sup> and intensity-modulated photovoltage spectroscopy (IMVS)<sup>[9,10]</sup> have been extensively used for this purpose.

These three techniques were developed independently and their results are often analyzed with different procedures, thus limiting the information that can be obtained from the characterization. IS data are generally analyzed with an equivalent circuit (EC), where the internal processes are modeled with passive electrical elements such as resistances, capacitances, and inductances.<sup>[11,12]</sup> On the other hand, IMPS and IMVS data are usually limited to the analysis of the characteristic times.<sup>[13,14]</sup>


The combination of the three techniques has gained interest in recent years, exposing the intrinsic relationship among them. However, their experimental application has been challenging.<sup>[15,16]</sup> One of the first attempts to combine IS, IMPS, and IMVS for the analysis of electrochemical systems was made by Klotz et al. They studied the charge carrier dynamics in hematite photoanodes using a distribution of relaxation times.<sup>[17]</sup> This procedure can be particularly useful to separate polarization processes, but its implementation is not straightforward, particularly in complex systems. Bertoluzzi and Bisquert proposed an EC for a water-splitting system, reporting the corresponding simulated spectra for IS, IMPS, and IMVS.<sup>[18]</sup> Subsequently, Ravishankar

## 1. Introduction

Photoconversion devices, including photovoltaic and photoelectrochemical cells, are gaining increasing attention over time,

A. O. Alvarez, L. Montañés, E. Mas-Marzá, S. Giménez, F. Fabregat-Santiago  
Institute of Advanced Materials  
Universitat Jaume I  
12006 Castellón de la Plana, Spain  
E-mail: agalvare@uji.es; fabresan@uji.es

M. García-Tecedor  
Photoactivated Processes Unit  
IMDEA Energy Institute  
28935 Móstoles, Spain

 The ORCID identification number(s) for the author(s) of this article can be found under <https://doi.org/10.1002/solr.202200826>.

© 2022 The Authors. Solar RRL published by Wiley-VCH GmbH. This is an open access article under the terms of the Creative Commons Attribution-NonCommercial-NoDerivs License, which permits use and distribution in any medium, provided the original work is properly cited, the use is non-commercial and no modifications or adaptations are made.

DOI: 10.1002/solr.202200826

et al. proposed an EC to fit the IS and the IMPS responses of a perovskite solar cell, although some discrepancies were observed between both results.<sup>[19]</sup> Following these results, we have recently proposed an improved characterization procedure by combining the three techniques, for a generic photoconversion device. This procedure was applied to analyze the response of a silicon photodiode using a common model for IS, IMPS, and IMVS. This combination proved to maximize the information obtained from the device, both qualitatively and quantitatively and at the same time allows accessing new information that cannot be obtained using the techniques individually.<sup>[20]</sup>

In that previous work, it is considered that photogeneration can be separated from the other processes in the device. This can be appropriate for many systems, as exemplified with a silicon photodiode. However, there are other systems where photogeneration is distributed within a space where transport and recombination may also be nonuniform. This is the scenario of more complex systems, such as distributed photogeneration in a thin film with coupled diffusion and recombination. These processes determine the performance of many photoconversion devices, including photovoltaic devices such as dye-sensitized solar cells,<sup>[21]</sup> perovskite solar cells<sup>[22]</sup>; and photoelectrochemical devices,<sup>[23]</sup> so their understanding is key to optimizing the system behavior.

IS was widely used to characterize such devices, allowing the extraction of quantitative parameters such as diffusion length and recombination frequency.<sup>[12,23–25]</sup> These applications were widespread by the developments made mainly by Bisquert and co-workers, which include the determination of the IS transfer function from fundamental equations and the presentation of the corresponding EC.<sup>[26–28]</sup> Although these developments have shown to be a game-changer in the characterization of optoelectronic devices, in some cases, the IS spectra are not clear enough to characterize properly the diffusive process.<sup>[29]</sup> Even when the analysis is possible, there are intrinsic limitations such as identifying if the diffusive carriers are electrons, holes, or even ions.

Similarly, the IMPS transfer function was also deduced from fundamental equations. This theoretical development was mainly carried out by Peter and his co-workers. These authors also showed the experimental application in dye-sensitized solar cells.<sup>[21]</sup> Recently, this development was also experimentally applied to analyze the IMPS response of a perovskite solar cell.<sup>[22]</sup> Following these theoretical equations, the IMVS transfer function was also developed from fundamental equations.<sup>[30]</sup> Finally, the three transfer functions were deduced from a proposed EC for dye-sensitized solar cells, including other internal processes.<sup>[31,32]</sup> However, this EC has not been used for the practical analysis of devices combining IS, IMPS, and IMVS spectra, yet.

In this work, we will show that it is possible to combine IS, IMPS, and IMVS techniques to improve the characterization of systems with distributed photogeneration, diffusion, and recombination processes. We will consider a general theoretical framework for these devices, from which the transfer functions are derived. Simulations of these transfer functions will be discussed to describe the possible spectra expected for these processes. Finally, this information will be used for the practical characterization of a water oxidation photoelectrode, with zircon-doped BiVO<sub>4</sub> (Zr:BiVO<sub>4</sub>) as an active layer.

While Zr:BiVO<sub>4</sub> is a promising photoanode material for water splitting,<sup>[33–36]</sup> it also suffers from poor charge transport, slow

water oxidation kinetics, and high surface recombination.<sup>[37,38]</sup> We will show that our methodology can help in understanding these internal processes behind performance losses, improving previous approaches used to investigate these electrodes,<sup>[17,39,40]</sup> including the separate use of IS,<sup>[41–44]</sup> IMPS,<sup>[45–49]</sup> and IMVS.<sup>[50–52]</sup>

## 2. Theory: Transfer Functions

Figure 1a illustrates the basic light conversion mechanism occurring in a photoconversion device, where the photogeneration is distributed over the light absorber layer (AL), and the charges must diffuse to be extracted, whilst recombination can take place along the layer. As depicted, when a photon flux ( $\phi$ ) reaches the device, only part of the photons will reach the absorber material ( $\phi_{\text{int}} = \eta_{\text{opt}}\phi$ , with  $\eta_{\text{opt}}$  the optical efficiency) and the rest will be lost, for example, by reflectance at the contacts. The absorbed current can be defined by  $j_a = qa\phi_{\text{int}}$ , where  $q$  is the elementary charge and  $a = e^{-\alpha d}$ , the absorbance, is the fraction of  $\phi_{\text{int}}$  that generates electron-hole pairs, where  $\alpha$  is the absorption coefficient and  $d$  is the thickness of the absorber. The pairs can be successfully separated in the active material to generate free-photogenerated charges in the AL ( $j_{\text{ph}} = \eta_{\text{sep}}j_a$ , with  $\eta_{\text{sep}}$  as the separation efficiency). Depending on whether the illumination is incident from the ES or the HS, the position-dependent probability of generating free charges can be expressed as

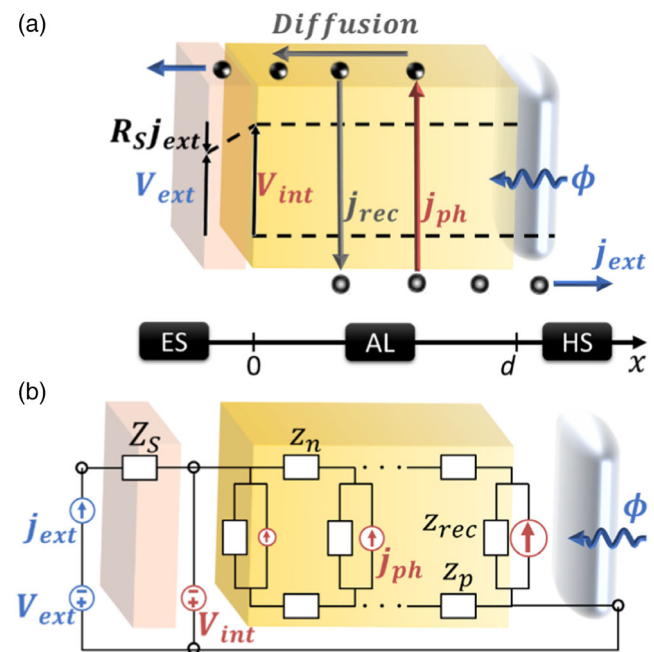


**Figure 1.** a) Scheme of the basic processes occurring in a photoconversion device with distributed photogeneration, recombination, and diffusion. AL is the light absorber layer with thickness  $d$ , while ES and HS are the electron- and hole-collector sides, respectively.  $\phi$  is the photon flux,  $j_{\text{ph}}$ ,  $j_{\text{rec}}$  and  $j_{\text{ext}}$  are the free-photogenerated, recombination and extracted currents, respectively.  $V_{\text{app}}$  is the externally applied voltage,  $V_{\text{int}}$  the internal voltage in the film, and  $R_s$  is a series resistance. b) EC modeling the device schematized in a), where  $z_n$  and  $z_p$  are impedance per unit length, while  $z_{\text{rec}}$  is an impedance length.  $Z_s$  is a series impedance, illustrated here on the ES layer, but it can contain other processes such as transport in the HS layer and interfacial processes.

$$G^{\text{HS}}(x) = \eta_{\text{sep}} \eta_{\text{opt}} \alpha \varphi e^{\alpha(x-d)} \quad (1)$$

$$G^{\text{ES}}(x) = \eta_{\text{sep}} \eta_{\text{opt}} \alpha \varphi e^{-\alpha x} \quad (2)$$

Then, the diffusion of the carriers toward the contacts takes place. During the diffusion, part of the carriers is lost as recombination current ( $j_{\text{rec}}$ ), which depends on the internal voltage ( $qV_{\text{int}} = E_{\text{Fn}} - E_{\text{Fp}}$ ). The charges that reach the contact and are successfully extracted generate the extracted current ( $j_{\text{ext}} = j_{\text{ph}} - j_{\text{rec}} = \eta_{\text{col}} j_{\text{ph}}$ , with  $\eta_{\text{col}}$  the collection efficiency). Therefore, the current that is extracted from the device can be written as

$$j_{\text{ext}} = q a \eta_{\text{col}} \eta_{\text{sep}} \eta_{\text{opt}} \varphi \quad (3)$$

Which is a function of  $V_{\text{int}}$  which is determined by the externally applied (or measured) voltage ( $V_{\text{ext}} = V_{\text{int}} + R_s j_{\text{ext}}$ ).

Note that in literature there is a variety in the notation of the variables involved in this article, which may become an obstacle for the follow-up and comparison of publications. In Supporting Information (SI), we present Table S1, with a summary of the notations used on some relevant papers in the field to ease help with this problem.

To apply any of the small perturbation techniques (IS, IMPS, or IMVS) to a specific device, a steady-state condition is needed. In addition, the combination of IS, IMPS, or IMVS for a complementary analysis imposes that these three small perturbation techniques are applied in the same steady-state condition. The steady-state conditions are defined by the light ( $\bar{\varphi}$ ), applied voltage ( $\bar{V}_{\text{ext}}$ ), and extracted current ( $\bar{j}_{\text{ext}}$ ), where the variables with overbars ( $\bar{\phantom{x}}$ ) indicate DC signals. In particular, to measure IS, an AC small-perturbation in voltage ( $\tilde{V}_{\text{ext}}$ ) is applied and the corresponding AC extracted current density ( $\tilde{j}_{\text{ext}}$ ) is measured, where the variables with a tilde ( $\tilde{\phantom{x}}$ ) indicate AC perturbations. The IS transfer function is defined by

$$Z = - \frac{\tilde{V}_{\text{ext}}}{\tilde{j}_{\text{ext}}} \quad (4)$$

Here, the sign of the current is a convention. In the case of IS, the current is usually considered positive when it flows into the device. In our case, we denoted this convention as the injected current ( $\tilde{j}_{\text{inj}} = -\tilde{j}_{\text{ext}}$ ).<sup>[20,53]</sup>

Similarly, to measure IMPS or IMVS, a small perturbation is applied in the light ( $\tilde{\varphi}$ ) and the  $\tilde{j}_{\text{ext}}$  or  $\tilde{V}_{\text{ext}}$  responses are measured, respectively. The corresponding transfer functions are defined by

$$Q = \frac{\tilde{j}_{\text{ext}}}{q \tilde{\varphi}} \quad (5)$$

$$W = \frac{\tilde{V}_{\text{ext}}}{q \tilde{\varphi}} \quad (6)$$

Note that from Equation (3) it may be deduced that a small perturbation of the photon flux provides  $\tilde{j}_{\text{ext}} = q a \eta_{\text{col}} \eta_{\text{sep}} \eta_{\text{opt}} \tilde{\varphi}$ , which is key for relating the parameters obtained from IS, IMPS, and IMVS.<sup>[20]</sup>

From the definitions of the transfer functions, the relationship

$$W = Z \times Q \quad (7)$$

emerges intuitively. This relationship has been explored theoretically in multiple studies,<sup>[18,20,32]</sup> but experimentally it has been shown that this is not always fulfilled.<sup>[15,16,29]</sup> Therefore, we emphasize the importance of verifying this relationship for each case under study, before combining the three techniques.<sup>[20,32]</sup>

## 2.1. Transmission Line Equivalent Circuit

Figure 1b shows a transmission line-based EC for the analysis of the device schematized in Figure 1a.  $z_n = Z_n/d$  and  $z_p = Z_p/d$  are impedance per unit length, accounting respectively for the electron and hole transport processes within the AL. On the other hand,  $z_{\text{rec}} = Z_{\text{rec}}d$  is an impedance length accounting for interaction processes between these two species, such as recombination and accumulation.  $Z_s$  is a series impedance, illustrated in Figure 1b as the ES layer impedance, although  $Z_s$  can account for alternative processes such as transport in the HS layer as well as interfacial processes. The acquisition of the IS, IMPS, and IMVS transfer functions from a simpler EC was exposed in our previous work,<sup>[20]</sup> and despite the current complexity, the basic idea to obtain the transfer functions is similar. As explained above,  $\tilde{\varphi} = 0$  when IS is measured, which is equivalent to removing  $j_{\text{ph}}$  from the EC (Figure 1b). Then, from the simplified EC, the impedance of the transmission line was solved in previous works,<sup>[54,55]</sup> and we reformulate it as

$$Z_{\text{D-R}} = \frac{\tilde{V}_{\text{int}}}{\tilde{j}_{\text{inj}}} = \frac{Z_n Z_p}{Z_n + Z_p} \left( 1 + \frac{2}{\Gamma \sinh(\Gamma)} \right) + \frac{Z_n^2 + Z_p^2 \coth(\Gamma)}{Z_n + Z_p \Gamma} \quad (8)$$

where

$$\Gamma = \sqrt{\frac{Z_n + Z_p}{Z_{\text{rec}}}} \quad (9)$$

is a dimensionless parameter related to the effective constraints on charge extraction (or injection), tending to zero when the transport impedances ( $Z_n$  and  $Z_p$ ) do so, as well as when the recombination impedance ( $Z_{\text{rec}}$ ) tends to infinity.

Finally, considering the effect of  $Z_s$ , the IS transfer function is

$$Z = Z_s + Z_{\text{D-R}} \quad (10)$$

Similarly, considering the effect of the conversion parameters from irradiance to the photogeneration,<sup>[19]</sup> provided by Equation (3) and the resulting distributed photogeneration ( $j_{\text{ph}}$ ) on the EC, together with the IMPS and IMVS transfer functions solved in previous works,<sup>[30–32]</sup> we can obtain

$$Q = \frac{\eta_{\text{opt}} \eta_{\text{sep}} (\eta_{\text{r}}^n Z_n + \eta_{\text{r}}^p Z_p) (Z_n + Z_p)}{[Z_s (Z_n + Z_p) + Z_n Z_p] \frac{\Gamma}{\coth(\Gamma)} + \frac{2Z_n Z_p}{\cosh(\Gamma)} + Z_n^2 + Z_p^2} \quad (11)$$

$$W = \eta_{\text{opt}} \eta_{\text{sep}} [\eta_{\text{r}}^n Z_n + \eta_{\text{r}}^p Z_p] \frac{\coth(\Gamma)}{\Gamma} \quad (12)$$

These transfer functions are written as a function of impedance parameters ( $Z$ ,  $\Gamma$ ), optical elements ( $\eta_{\text{opt}}$ ,  $\eta_{\text{sep}}$ ), and mixed elements as  $\eta_{\Gamma}^n$  and  $\eta_{\Gamma}^p$ . The specific definition of  $\eta_{\Gamma}$  depends on whether the illumination is from HS or ES

$$\eta_{\Gamma}^{n,\text{HS}} = \eta_{\Gamma}^{p,\text{ES}} = \frac{(a-1)\left(1 + \frac{\Gamma}{A} \tanh(\Gamma)\right) + \frac{1}{\cosh(\Gamma)}}{1 - \frac{\Gamma^2}{A^2}} \quad (13)$$

$$\eta_{\Gamma}^{p,\text{HS}} = \eta_{\Gamma}^{n,\text{ES}} = \frac{1 - \frac{\Gamma}{A} \tanh(\Gamma) + \frac{a-1}{\cosh(\Gamma)}}{1 - \frac{\Gamma^2}{A^2}} \quad (14)$$

where  $A = -\log(1-a) = \alpha d$  is the absorbance and the superscripts  $n$  and  $p$  denote electrons and holes, respectively. Figure S1, Supporting Information, shows the possible values that can be taken for these functions in the low-frequency limit ( $\omega \rightarrow 0$ ). As can be noted,  $\eta_{\Gamma}$  is equal to  $a$  when  $\Gamma = 0$  and it decreases as  $\Gamma$  increases.

Writing the transfer functions  $Z$ ,  $Q$  and  $W$  using the same parameters is key, as it allows the simultaneous analysis of experimental data.

## 2.2. Single-Carrier Diffusion

In this section, it will be considered that only one species (e.g., electrons) limits the performance of a device, which implies that the other species (holes in this case) are more efficiently extracted. In this case, the electron carrier density ( $n$ ) can be described by

$$\frac{dn}{dt} = D \frac{d^2n}{dx^2} - \frac{n}{\tau_{\text{rec}}} + G(x, t) \quad (15)$$

where  $D$  is the diffusion coefficient and  $\tau_{\text{rec}}$  is the lifetime of the diffusion carriers. The case where the diffusive carriers are holes ( $p$ ) instead of electrons ( $n$ ) is described by the same equation. The differences between these two cases are the boundary conditions, as shown in Section S1 in the Supporting Information.

In the case of IS,  $G(x, t)$  is eliminated in Equation (15) and the IS transfer function is

$$Z_{\text{D-R}} = R_{\text{tr}} \coth(\Gamma) / \Gamma \quad (16)$$

as previously obtained by Bisquert.<sup>[26]</sup> with

$$\Gamma = \sqrt{\frac{\omega_{\text{rec}} + i\omega}{\omega_{\text{D}}}} \quad (17)$$

where  $\omega_{\text{rec}} = 1/\tau_{\text{rec}}$  and  $\omega_{\text{D}} = D/d^2$  are the recombination and diffusion frequencies, and  $R_{\text{tr}}$  is defined as the diffusion resistance.

Finally, if it is considered that the series impedance is a single-series resistance ( $R_{\text{S}}$ ), the total (measurable) impedance becomes

$$Z = R_{\text{S}} + Z_{\text{D-R}} \quad (18)$$

The effect of incorporating a series resistance modifies the IMPS and IMVS transfer functions obtained from Equation (15) providing<sup>[9,22,29,30]</sup>

$$Q = \eta_{\text{opt}} \eta_{\text{sep}} \eta_{\Gamma} \left[ 1 + \frac{R_{\text{S}}}{Z_{\text{D-R}}} \right]^{-1} \quad (19)$$

$$W = \eta_{\text{opt}} \eta_{\text{sep}} \eta_{\Gamma} Z_{\text{D-R}} \quad (20)$$

where  $\eta_{\Gamma}$  is defined by Equation (13) or (14) depending on whether the diffusing species are electrons or holes and whether the illumination is from HS or ES.

The EC corresponding to Equations (18), (19) and (20) is shown in Figure 2a, which is a particular case of the EC in Figure 1b (see more details in Section S3 of the Supporting Information). This EC provides the following equivalences: for the transport resistance  $R_{\text{tr}} = r_{\text{tr}} d$ , for the recombination resistance  $R_{\text{rec}} = r_{\text{rec}}/d = R_{\text{tr}} \omega_{\text{D}} \tau_{\text{rec}}$ , and for the chemical capacitance  $C_{\mu} = c_{\mu} d = 1/R_{\text{rec}} \omega_{\text{rec}}$ . The diffusion length is key to explaining carrier collection in photoelectrochemical devices and can be obtained from the parameters provided though  $L = d \sqrt{\omega_{\text{D}} \tau_{\text{rec}}} = d \sqrt{R_{\text{rec}}/R_{\text{tr}}}$ .<sup>[12,27]</sup> With these definitions, Equation (17) provides that at the low-frequency limit  $\Gamma(\omega \rightarrow 0) = d/L$ . Note that for good carrier collectors  $L/d \gg 1$ , which implies that at the low-frequency limit  $\Gamma \rightarrow 0$ .

Considering explicitly the optical efficiency, the differential external and internal quantum efficiencies can be expressed as<sup>[20,56]</sup>

$$\text{EQE}_{\text{PV-Diff}} = a \eta_{\text{sep}} \eta_{\text{col}} \eta_{\text{opt}} \quad (21)$$

$$\text{IQE}_{\text{PV-Diff}} = \frac{\text{EQE}_{\text{PV-Diff}}}{\eta_{\text{opt}} a} \quad (22)$$

$\text{EQE}_{\text{PV-Diff}}$  corresponds to the low-frequency limit of  $Q$ . Then, comparing Equation (19) and (21), we have

$$\eta_{\text{col}} = \frac{\eta_{\Gamma}(\omega \rightarrow 0)}{a} \left[ 1 + \frac{R_{\text{S}}}{Z_{\text{D-R}}(\omega \rightarrow 0)} \right]^{-1} \quad (23)$$

This equation points out the dependence of  $\text{EQE}_{\text{PV-Diff}}$  and thus  $\text{IQE}_{\text{PV-Diff}}$ , on the diffusion length (through  $\eta_{\Gamma}$ ),<sup>[57]</sup> but also on the ratio between the series resistance and the low-frequency limit of  $Z_{\text{D-R}}$ .

At this point is worthwhile to mention that the three transfer functions theoretically obtained comply with the relationship given in Equation (7), in all the scenarios presented in this study. Therefore, the parameters obtained from the fitting of experimental data should be the same for the three modulated techniques.

## 3. Simulation of Transfer Functions

Figure 2b shows a typical spectrum of the IS response of the EC in Figure 2a, given by Equation (18). It is important to highlight that the shape of the IS spectrum is independent of parameters such as the absorbance ( $a$ ), the illumination side, and even the carrier species (electrons or holes), as long as the resistances ( $R_{\text{tr}}$ ,  $R_{\text{rec}}$ , and  $R_{\text{S}}$ ) and the characteristic frequencies ( $\omega_{\text{rec}}$  and  $\omega_{\text{D}}$ ) are kept constant.

Figure 2c-f shows the IMPS and IMVS simulations of Equation (19) and (20) for different absorbances. Considering HS illumination and electron diffusion and recombination, a characteristic feature is observed for the IMPS and IMVS

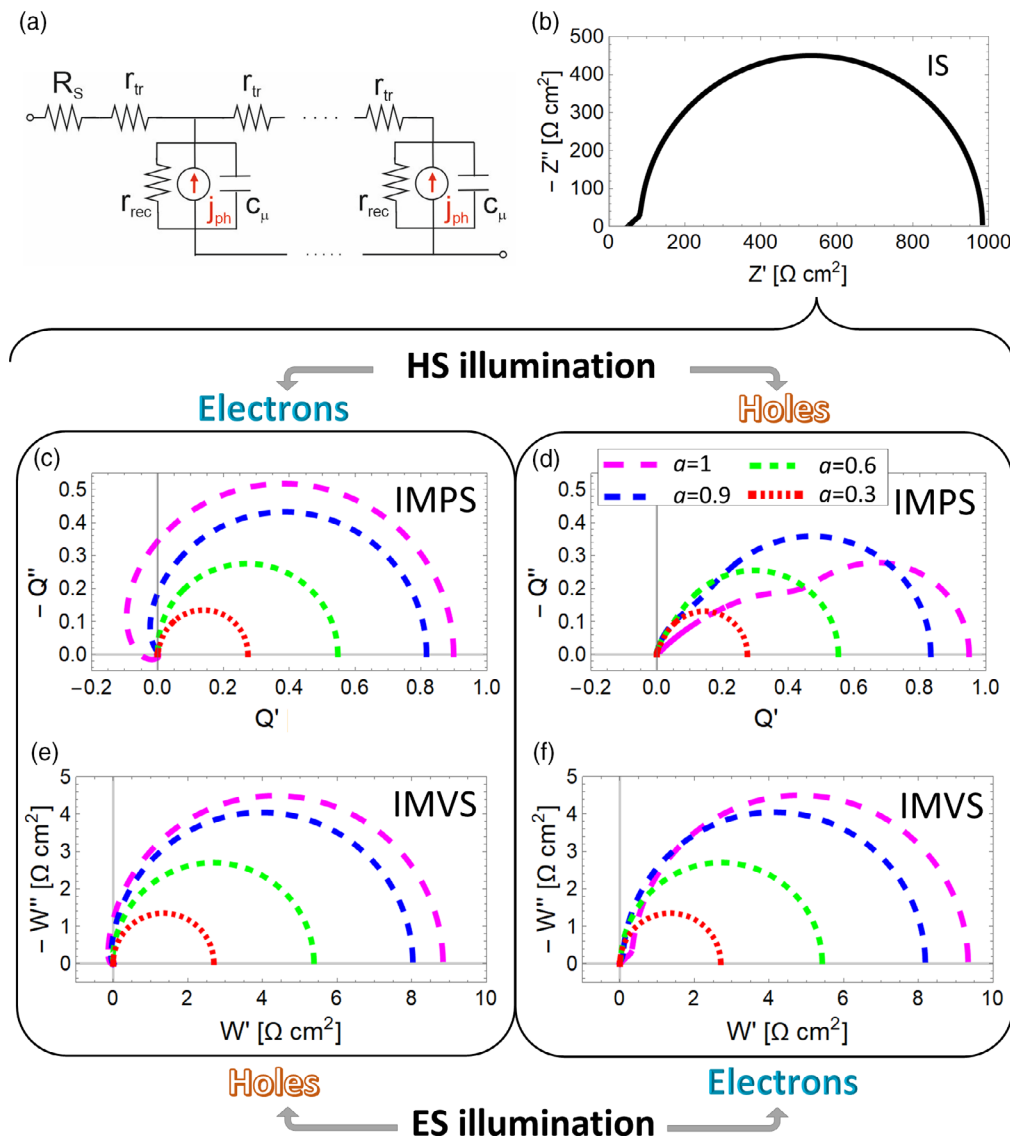


**Figure 2.** a) EC model for single-carrier transport and recombination with distributed absorption, used to simulate b) IS, c,d) IMPS, and e,f) IMVS spectra, with  $R_S = 50 \Omega \text{ cm}^2$ ,  $R_{tr} = 100 \Omega \text{ cm}^2$ ,  $\omega_D = 450 \text{ rad s}^{-1}$ ,  $\omega_{rec} = 50 \text{ rad s}^{-1}$ , and  $\eta_{sep}\eta_{opt} = 100\%$ . Consider either electrons or holes as diffusing species, with light reaching the device from the “ES” and “HS,” respectively. The different plots represented in IMVS and IMPS correspond to different absorptance ( $a$ ) as indicated in the legend.

responses (Figure 2c,e):  $Q'$  and  $W'$  reach negative values at high frequencies. In contrast, for the same HS illumination, but for hole diffusion and recombination, the IMPS and IMVS spectra (Figure 2d,f) do not present this characteristic feature. For this case, these spectra are more similar to the IS spectrum (Figure 2b), especially the IMVS spectrum. The electron and hole responses for ES illumination are inverted from those obtained for HS illumination. Thus, the diffusion and recombination of holes produce the spectra with  $Q'$  and  $W'$  entering the negative region at high frequencies (Figure 2c,e), while for the electrons this feature is not present (Figure 2d,f).

The effect of the decrease of  $a$  is clear in both IMPS simulations (Figure 2c,d), mainly reducing the value of the low-frequency limit, as expected because this limit is the

$\text{EQE}_{\text{PV-Diff}}$ , see Equation (21).<sup>[20,56]</sup>  $a$  has a similar effect on the IMVS simulations (Figure 2e,f), as expected as the IS spectrum is independent of  $a$ , see Equation (7).

One of the most interesting results of Section 2.1 is that, when both electrons and holes are diffusing, the IMVS transfer function, Equation (12), is the combination of both  $\eta_{tr}^n$  and  $\eta_{tr}^p$ , weighed by  $Z_n$  and  $Z_p$ , respectively. From a practical point of view, this means that the IMVS spectra will be the sum of both Figure 2e,f, multiplied by the electron and hole transport resistances, respectively. Something equivalent accounts for the IMPS spectra. This observation allows a qualitative characterization to identify the dominant diffusive species, by observing the IMPS and IMVS spectra, particularly if one of these resistances is much smaller than the other.

#### 4. Results

In this section, we combine IS, IMPS and IMVS to characterize the optoelectronic properties of a porous Zr:BiVO<sub>4</sub> electrode used in a photoelectrochemical cell for water oxidation. **Figure 3** shows the cyclic voltammetry curves without illumination (black line) and under blue illumination (470 nm at 89 mW cm<sup>-2</sup>, blue lines), for ES (solid lines) and HS (dashed lines) illumination. In this device, the ES illumination corresponds to illumination from the FTO side, while the HS illumination corresponds to illumination from the electrolyte side. Figure S2, Supporting Information, compares these measurements with the measurements made under 1 sun illumination (yellow lines). Under blue illumination, a higher  $j_{\text{ext}}$  is obtained since almost all the light is absorbed by the material (see Figure S3, Supporting Information). Regardless of illuminating with 1 sun or with blue light, a higher  $j_{\text{ext}}$  is obtained for ES illumination, in good agreement with previous studies in BiVO<sub>4</sub> photoanodes.<sup>[58]</sup> We will show that the characterization combining IS, IMPS and IMVS allows a deep understanding of the operating processes and the differences between ES and HS lighting. In this work, we have performed this characterization under the same blue light illumination at 1.2 V versus Reversible Hydrogen Electrode (RHE) (gray line in Figure 3) and in the presence of 0.1 M Na<sub>2</sub>SO<sub>3</sub> as hole scavenger in 0.1 M KPi buffer (pH = 7.5).

**Figure 4** shows (solid black circles) the IS, IMPS, and IMVS measured spectra of the Zr:BiVO<sub>4</sub> photoelectrochemical cell, exposed to HS illumination (a, c, and e, respectively) and ES illumination (b, d, and f, respectively). In all spectra the frequency range is from 5 kHz to 1 Hz. In Figure 4e,f, the comparison of  $W$  with the product of  $Z$  and  $Q$  (see Equation (7)) is presented

(empty red squares). In general, the experimental data are in good agreement with Equation (7). The major difference between  $W$  with the product of  $Z$  and  $Q$  is observed at lower frequencies, but this is not a limitation for our analysis because we are interested in the processes taking place at high frequencies. For this reason, we will focus on the experimental data until 20 Hz for our analysis.

Independently of the illumination side, the shapes of IS, IMVS and IMPS spectra (Figure 4), exhibit the same features, presenting the characteristic trend, reaching negative values at high frequencies for  $Q'$  and  $W'$ . The main differences between the experimental spectra for the different illumination sides relate to the low-frequency values obtained for IS and IMPS, which correspond to total resistance and the EQE<sub>PV-Diff</sub>, respectively.<sup>[20,56]</sup> Comparing Figure 4 with 2 is not surprising that the experimental IS spectra are similar, since this technique gives the same response for the different scenarios. However, by comparing the experimental IMPS and IMVS spectra in Figure 4 with the simulations in Figure 2, we can conclude that the extraction of electrons determines the device performance when the illumination reaches the device from the HS, while when the illumination is from the ES, the limiting carriers are the holes. This means that the other carrier species (holes for HS illumination and electrons for ES illumination) are transported well enough to have no significant effect on the IMPS and IMVS spectra, see Equation (12) and the corresponding discussion in Section 3. These results could be attributed to the fact that the carriers that dominate the spectral response have to travel longer distances as they are, on average, generated farther away from their extracting contact, while the other species can be more easily extracted.

Therefore, we analyzed all the experimental spectra with the EC in Figure 2a, whose transfer functions are given by Equation (18) and (16) for IS, and Equation (19) and (20) for IMPS and IMVS, restricted to  $\eta_{\text{T}}$  given by Equation (13). We used these equations to fit simultaneously the three measurements (IS, IMPS, and IMVS), using Wolfram Mathematica software. The fitting results are shown as blue lines in Figure 4, having an excellent match with the experimental results. The extracted parameters, with variable errors below 10% and  $R^2$  values above 0.999, are presented in Table S2, Supporting Information and summarized in **Table 1**.

Comparing the parameters from the fitting of each illumination side in Table 1, we can first notice that the  $R_s$  values are practically identical, these resistances corresponding to the high-frequency limit of Figure 4a,b. This is an expected result because this quantity is associated with transport properties external to the AL, which should be, in principle, independent of the illumination conditions.

Data obtained from the fitting of measurements with ES and HS illuminations indicate that the holes are transported more efficiently than the electrons, as they have a considerably lower  $R_{\text{tr}}$ , higher  $\omega_{\text{D}}$ , and consequently, a higher diffusion coefficient. In contrast,  $\omega_{\text{rec}}$  of holes almost doubles that of electrons, which implies that they have almost half the lifetime of electrons. While chemical capacitance is similar, a bit larger for holes, the large difference in  $\omega_{\text{rec}}$  is associated with the large difference observed in recombination resistance, which is much smaller for holes, indicating larger recombination. As consequence, the diffusion

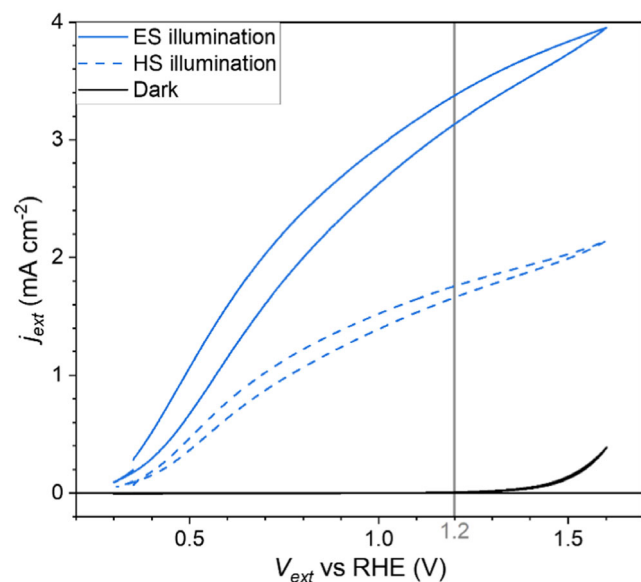


**Figure 3.** Cyclic voltammetry curves of a Zr:BiVO<sub>4</sub> electrode used in water-splitting photoelectrochemical cell: without illumination (black line) and 89 mW cm<sup>-1</sup> of blue light (blue lines); from the ES, continues lines, and the HS, dashed lines. IS, IMPS, and IMVS are measured under the same illumination conditions and at 1.2 V versus RHE (gray line).

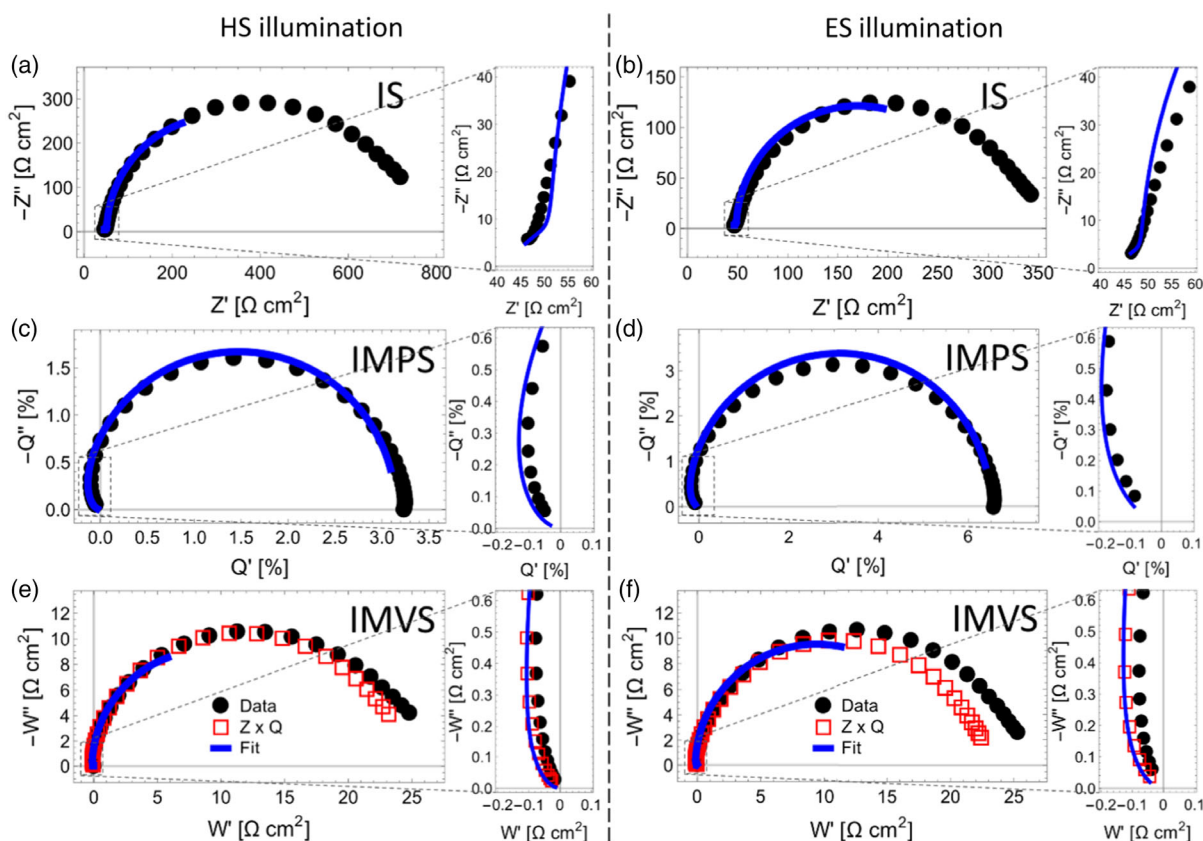


**Figure 4.** a) IS, c) IMPS, and e) IMVS (with their respective zooms) measurement results (solid black circles) of a Zr:BiVO<sub>4</sub> electrochemical cell illuminated from the HS (see Figure 1). The spectra in b, d, and f show the corresponding measurements for ES illumination. In (e,f) measured  $W$ s are compared  $W$  with the product of  $Z$  and  $Q$  (see Equation (7)), in red empty squares. The blue lines represent the simultaneous fittings of each set of measurements (IS, IMPS, and IMVS), with the EC in Figure 2a. The measurements were performed at 89 mW cm<sup>-2</sup> blue light (470 nm) and 1.2 V versus RHE. The frequency range is, in all the spectra, from 5 kHz to 1 Hz.

**Table 1.** Resulting parameters from the simultaneous fitting of the IS, IMPS and IMVS spectra for both HS and ES illumination in Figure 4, with the EC in Figure 2a and  $\alpha = 98\%$  obtained from direct measurement.

Illumination	HS	ES
Diffusion Species	Electrons	Holes
$R_S$ [ $\Omega$ cm <sup>2</sup> ]	41.3 ± 0.2	43.2 ± 0.1
$R_{tr}$ [ $\Omega$ cm <sup>2</sup> ]	31 ± 2	16.4 ± 0.4
$D$ [cm <sup>2</sup> s <sup>-1</sup> ]	(3.7 ± 0.3) × 10 <sup>-6</sup>	(5.7 ± 0.2) × 10 <sup>-6</sup>
$\omega_{rec}$ [rad s <sup>-1</sup> ]	87 ± 4	155 ± 3
$R_{rec}$ [ $\Omega$ cm <sup>2</sup> ]	520 ± 50	240 ± 10
$C_\mu$ [ $\mu$ F cm <sup>-2</sup> ]	22 ± 2	27 ± 1
$L$ [ $\mu$ m]	2060 ± 70	1920 ± 30
$\eta_{col}$ [%]	90 ± 4	83 ± 2
$\eta_{sep}$ [%]	4.4 ± 0.2	10.9 ± 0.2
IQE <sub>PV-Diff</sub> [%]	4.0 ± 0.2	8.8 ± 0.3
EQE <sub>PV-Diff</sub> [%]	3.1 ± 0.1	6.5 ± 0.1

length,  $\approx 4$  times the film thickness, is very similar in the two cases, slightly larger for the electrons.

These results are consistent with previous studies. In fact,  $\omega_{rec}$  has been measured for BiVO<sub>4</sub> photoanodes using IMPS, achieving values around 100 rad s<sup>-1</sup>, which are in good agreement with the values reported in Table 1.<sup>[45,59]</sup>  $D$  is proportional to the carrier mobility ( $\mu$ ) through the equation  $D = kT\mu/q$ , whereby we obtained electron and hole mobility values of  $1.4 \times 10^{-4}$  and  $2.2 \times 10^{-4}$  cm<sup>2</sup> V<sup>-1</sup> s<sup>-1</sup>, respectively (see Table S2, Supporting Information). Similar values were reported by Abdi and coworkers for the mobility of W-doped BiVO<sub>4</sub>, suggesting that Zr and W doping could have a similar effect on the photoanode. Furthermore, in that work, lower mobility values for HS illumination ( $\approx 30\%$ ) were also reported.<sup>[60]</sup> However, the corresponding characteristic times in that article were in the ns order, which yields diffusion lengths in the nm order, which in our case would yield to the impossibility of collecting current because our thickness is several orders of magnitude greater. Those measurements were performed on films, without selective contacts, and this difference could be the reason for a much shorter carrier lifetime than the one presented in Table 1.

Table 1 shows, in both cases, that  $\eta_{col}$  is smaller than 100%, which is the value usually considered under hole scavenger conditions (the present case).<sup>[23]</sup> For illumination from the ES,  $\eta_{col}$  is smaller than from HS, in good agreement with diffusion length.

This result might suggest a smaller  $j_{\text{ext}}$  for ES illumination which is contrary to the experimental measurements (Figure 3). The reason for this behavior is that, as shown in Table 1, the charge separation efficiency for HS illumination is only 4.4% while for ES it reaches a value of 10.9%. Therefore, as the absorbance is 98% in both cases and the difference in the optical efficiency is very small (see Table S2 in Supporting Information), it can be concluded that the main limitation to extract absorbed current is  $\eta_{\text{sep}}$ . As a result, as shown in Equation (21), the  $\text{EQE}_{\text{PV-Diff}}$  is only 6.5% and 3.1% for ES and HS illumination, respectively, which is in line with the low-frequency limit of the IMPS spectra shown in Figure 3. Similar values have been reported in the literature for the EQE of these devices for blue light (470 nm).<sup>[23]</sup>

A possible origin of the differences between  $\eta_{\text{sep}}$  obtained in each case may be related to the presence of structural defects, mainly oxygen vacancies, on the surface of  $\text{BiVO}_4$ , as it has been extensively reported.<sup>[61–63]</sup> These defects can act as recombination centers, known as surface traps, that could ultimately decrease the  $\eta_{\text{sep}}$ .<sup>[64–66]</sup> Indeed, surface recombination was reported as the main limiting process on the performance of  $\text{BiVO}_4$  photoanodes.<sup>[45,67]</sup> When illuminating from the HS, the photogeneration is higher near this trap-rich interface which could act as an internal recombination center, thus reducing  $\eta_{\text{sep}}$ . Another possible origin is the higher conductivity found for holes which could help to separate carriers more efficiently. A more detailed analysis of the origin of the differences in  $\eta_{\text{sep}}$  is beyond the scope of this article and will be the target of future works.

In summary, we have shown here that the combination of the IS, IMPS, and IMVS measurements, followed by an appropriate analysis method, allows a detailed characterization of the optoelectronic processes in the  $\text{Zr:BiVO}_4$  photoanodes. This procedure can be used for the characterization of other photoconversion devices and electrodes, and it can be also extended for the analysis of the changes produced by varying the external voltage, the current, or the illumination conditions.

## 5. Conclusion

In this work, we establish the theoretical basis and a practical method for combining IS, IMPS, and IMVS to characterize photoconversion devices with distributed photogeneration, recombination and diffusion. The potential for this combination was demonstrated by comparing the possible responses of the three techniques for such devices. The practical application of this method is based on the simultaneous fitting of the experimental data, using the same model and parameters. The relationship between the optical and electrical properties is key for this analysis. The application of this method to a  $\text{Zr:BiVO}_4$  photoanode allowed, first, to identify the electrons as the carrier controlling the response of the device when the illumination arrives from the HS (the electrolyte), while the holes assume this role when the sample is illuminated from the ES (the FTO). Then, it provided a detailed quantitative characterization of the photoconversion parameters, that served to identify the separation efficiency as the main limitation to the performance of this device, which was 10.9% for ES and 4.4% for HS illumination. Other parameters, such as the recombination, transport resistance, diffusion

coefficient, and diffusion length of each carrier, played a minor role in the differences in device performance, including extracted current and external quantum efficiency found for each illumination side.

## 6. Experimental Section

$\text{Zr:BiVO}_4$  electrodes were prepared through a previously reported two-step method.<sup>[23,68]</sup> The first step was the electrodeposition of metallic Bi on fluorine-doped tin oxide (FTO,  $14 \Omega \text{sq}^{-1}$ )-coated glass substrate. The second step was the addition of the vanadium precursor by drop-casting technique. According to a previous optimization process, 2.5 mol% of  $\text{ZrCl}_2 \cdot 8\text{H}_2\text{O}$  (Sigma-Aldrich) was added to the  $\text{Bi}^{3+}$  plating bath.<sup>[69]</sup>

The optical properties were measured in a Lambda 1050+ spectrophotometer (Perkin Elmer), with  $\text{BaSO}_4$  as white reference. The optical efficiencies were calculated as

$$\eta_{\text{opt}}^{\text{HS}} = T_{\text{Quartz}}(1 - R_{\text{HS}}) \quad (24)$$

$$\eta_{\text{opt}}^{\text{ES}} = T_{\text{Quartz}}(1 - R_{\text{ES}})(1 - a_{\text{FTO}}) \quad (25)$$

where the superscript refers to the HS and ES illuminations,  $T_{\text{Quartz}}$  is the transmittance of the quartz cuvette,  $a_{\text{FTO}}$  is the absorbance of the FTO, and  $R_{\text{HS}}$  and  $R_{\text{ES}}$  are the reflectances of the measured film when light reaches from HS and ES, respectively. On the other hand, the absorbance ( $a$ ) was calculated by considering the photons that were not reflected or absorbed in the FTO.

$$a = 1 - \frac{T_{\text{HS}}}{1 - R_{\text{HS}}} \frac{1}{1 - a_{\text{FTO}}} \quad (26)$$

with  $T_{\text{HS}}$  the transmittance of the measured film when light reaches from HS. These variables are shown in Figure S3, Supporting Information.

The photoelectrochemical characterization of the electrodes was performed in the dark and under illumination ( $100 \text{ mW cm}^{-2}$  of white light and  $89 \text{ mW cm}^{-2}$  of blue light) in a 0.1 M Potassium phosphate buffer solution of pH 7.5, including 0.1 M  $\text{Na}_2\text{SO}_3$  solution as a hole scavenger. The electrochemical cell was composed of the working electrode, an  $\text{Ag/AgCl}$  (3 M KCl) reference electrode, and a Pt wire as a counter electrode. All the potentials were referred to the RHE through the Nernst equation

$$V_{\text{RHE}} = V_{\text{Ag/AgCl}} + V_{\text{Ag/AgCl}}^0 + 0.059 \text{pH} \quad (27)$$

where

$$V_{\text{Ag/AgCl}}^0 (3 \text{ m KCl}) = 0.199 \text{ V} \quad (28)$$

The IS, IMPS, and IMVS measurements were performed with an Autolab PGSTAT302 equipped with a FRA32M module and combined with the Light-emitting diode (LED) driver. The three techniques were measured under  $89 \text{ mW cm}^{-2}$  light intensity generated by an array of three blue LEDs (Philips LUMILEDS LXML-PB01-0040 with 470 nm peak). For the IS measurement, a 20 mV AC perturbation was applied. For IMPS and IMVS, an AC perturbation equal to 10% of the light flux was applied. The frequency range was for the three techniques from 5 kHz to 1 Hz. The measurements were performed at a bias voltage of 1.2 V versus RHE. The analysis of all spectra was done using MultiNonlinearModelFit function of Wolfram Mathematica software.

The morphology of the sample, including the thickness, was examined by field-emission scanning electron microscopy (FESEM) with a JSM-700F JEOL FEG-SEM system (Tokyo, Japan) equipped with an INCA 400 Oxford EDS analyzer (Oxford, UK) operating at 15 kV. Before the FESEM experiment, the samples were sputtered with a 2 nm-thick layer of Pt.



## Supporting Information

Supporting Information is available from the Wiley Online Library or from the author.

## Acknowledgements

This work has received funding from the European Union's Horizon 2020 MSCA Innovative Training Network MAESTRO under grant agreement No 764787. The authors thank support from project PID2020-116093RB-C41 funded by MCIN/AEI/10.13039/501100011033/ and from Generalitat Valenciana under the project PROMETEO/2020/028 for financial support. Dr. Ana Gutiérrez-Blanco and Serveis Centrals at UJI (SCIC) are also acknowledged for scanning electron microscopy characterization.

## Conflict of Interest

The authors declare no conflict of interest.

## Author Contributions

F.F.S. provided the original idea and supervised the research. A.O.A. carried out the calculations, simulations, experimental measurements, data analysis, and wrote the first version of the manuscript. L.M.G. fabricated the samples. F.F.S., E.M.M., M.G.T., and S.G. contributed to validating, reviewing, and editing the manuscript.

## Data Availability Statement

The data that support the findings of this study are openly available in [Experimental Data in "New Views on Carrier Diffusion and Recombination by Combining Small Perturbation Techniques: Application to BiVO<sub>4</sub> Photoelectrodes"] at [http://hdl.handle.net/10234/199215], reference number [199215].

## Keywords

BiVO<sub>4</sub>, impedance spectroscopy, intensity-modulated photocurrent spectroscopy, intensity-modulated photovoltage spectroscopy, water splitting

Received: September 8, 2022

Revised: October 8, 2022

Published online: November 3, 2022

- [1] J. H. Montoya, L. C. Seitz, P. Chakhranont, A. Vojvodic, T. F. Jaramillo, J. K. Nørskov, *Nat. Mater.* **2017**, *16*, 70.
- [2] M. G. Walter, E. L. Warren, J. R. McKone, S. W. Boettcher, Q. Mi, E. A. Santori, N. S. Lewis, *Chem. Rev.* **2010**, *110*, 6446.
- [3] A. O. Alvarez, R. Arcas, C. A. Aranda, L. Bethencourt, E. Mas-Marzá, M. Saliba, F. Fabregat-Santiago, *J. Phys. Chem. Lett.* **2020**, *11*, 8417.
- [4] N. Klipfel, A. O. Alvarez, H. Kanda, A. A. Sutanto, C. Igci, C. Roldán-Carmona, C. Mombiona, F. Fabregat-Santiago, M. K. Nazeeruddin, *ACS Appl. Energy Mater.* **2022**, *5*, 1646.
- [5] V. Babu, R. Fuentes Pineda, T. Ahmad, A. O. Alvarez, L. A. Castriotta, A. Di Carlo, F. Fabregat-Santiago, K. Wojciechowski, *ACS Appl. Energy Mater.* **2020**, *3*, 5126.
- [6] L. M. Peter, *Chem. Rev.* **1990**, *90*, 753.
- [7] S. Ravishankar, A. Riquelme, S. K. Sarkar, M. Garcia-Battle, G. Garcia-Belmonte, J. Bisquert, *J. Phys. Chem. C* **2019**, *123*, 24995.
- [8] A. Riquelme, F. E. Gálvez, L. Contreras-Bernal, H. Míguez, J. A. Anta, *J. Appl. Phys.* **2020**, *128*, 133103.
- [9] G. Schlichthörl, S. Y. Huang, J. Sprague, A. J. Frank, *J. Phys. Chem. B* **1997**, *101*, 8141.
- [10] R. Kern, R. Sastrawan, J. Ferber, R. Stangl, J. Luther, *Electrochim. Acta* **2002**, *47*, 4213.
- [11] F. Fabregat-Santiago, E. M. Barea, S. Giménez, J. Bisquert, in *Molecular Devices for Solar Energy Conversion and Storage*, (Eds: H. Tian, G. Boschloo, A. Hagfeldt), Springer Singapore, Singapore **2018**, 353.
- [12] J. Bisquert, F. Fabregat-Santiago, in *Dye-Sensitized Solar Cells* (Ed: K. Kalyanasundaram), CRC Press, Switzerland **2010**, p. 457.
- [13] E. Ponomarev, L. Peter, *J. Electroanal. Chem.* **1995**, *396*, 219.
- [14] L. M. Peter, *J. Solid State Electrochem.* **2013**, *17*, 315.
- [15] O. Almora, D. Miravet, G. J. Matt, G. Garcia-Belmonte, C. J. Brabec, *Appl. Phys. Lett.* **2020**, *116*, 013901.
- [16] O. Almora, Y. Zhao, X. Du, T. Heumueller, G. J. Matt, G. Garcia-Belmonte, C. J. Brabec, *Nano Energy* **2020**, *75*, 104982.
- [17] D. Klotz, D. S. Ellis, H. Dotan, A. Rothschild, *PCCP* **2016**, *18*, 23438.
- [18] L. Bertoluzzi, J. Bisquert, *J. Phys. Chem. Lett.* **2017**, *8*, 172.
- [19] S. Ravishankar, C. Aranda, S. Sanchez, J. Bisquert, M. Saliba, G. Garcia-Belmonte, *J. Phys. Chem. C* **2019**, *123*, 6444.
- [20] A. O. Alvarez, S. Ravishankar, F. Fabregat-Santiago, *Small Methods* **2021**, *5*, 2100661.
- [21] L. Dloczik, O. Ieperuma, I. Lauerma, L. Peter, E. Ponomarev, G. Redmond, N. Shaw, I. Uhlendorf, *J. Phys. Chem. B* **1997**, *101*, 10281.
- [22] A. Bou, H. Abolish, A. Ashoka, H. Cruanyes, A. Guerrero, F. Deschler, J. Bisquert, *ACS Energy Lett.* **2021**, *6*, 2248.
- [23] M. N. Shaddad, D. Cardenas-Morcoso, P. Arunachalam, M. Garcia-Tecedor, M. A. Ghanem, J. Bisquert, A. Al-Mayouf, S. Gimenez, *J. Phys. Chem. C* **2018**, *122*, 11608.
- [24] W. Choi, H.-C. Shin, J. M. Kim, J.-Y. Choi, W.-S. Yoon, *J. Electrochem. Sci. Technol* **2020**, *11*, 1.
- [25] W. Peng, C. Aranda, O. M. Bakr, G. Garcia-Belmonte, J. Bisquert, A. Guerrero, *ACS Energy Lett.* **2018**, *3*, 1477.
- [26] J. Bisquert, *J. Phys. Chem. B* **2002**, *106*, 325.
- [27] J. Bisquert, G. Garcia-Belmonte, F. Fabregat-Santiago, N. S. Ferriols, P. Bogdanoff, E. C. Pereira, *J. Phys. Chem. B* **2000**, *104*, 2287.
- [28] F. Fabregat-Santiago, J. Bisquert, G. Garcia-Belmonte, G. Boschloo, A. Hagfeldt, *Sol. Energy Mater. Sol. Cells* **2005**, *87*, 117.
- [29] A. Bou, A. Pockett, H. Cruanyes, D. Raptis, T. Watson, M. J. Carnie, J. Bisquert, *APL Mater.* **2022**, *10*, 051104.
- [30] J. Halme, K. Miettunen, P. Lund, *J. Phys. Chem. C* **2008**, *112*, 20491.
- [31] L. Bay, K. West, *Sol. Energy Mater. Sol. Cells* **2005**, *87*, 613.
- [32] J. Halme, *PCCP* **2011**, *13*, 12435.
- [33] T. W. Kim, K.-S. Choi, *Science* **2014**, *343*, 990.
- [34] J. Su, L. Guo, N. Bao, C. A. Grimes, *Nano Lett.* **2011**, *11*, 1928.
- [35] J. K. Cooper, S. Gul, F. M. Toma, L. Chen, P.-A. Glans, J. Guo, J. W. Ager, J. Yano, I. D. Sharp, *Chem. Mater.* **2014**, *26*, 5365.
- [36] A. Walsh, Y. Yan, M. N. Huda, M. M. Al-Jassim, S.-H. Wei, *Chem. Mater.* **2009**, *21*, 547.
- [37] W. Qiu, S. Xiao, J. Ke, Z. Wang, S. Tang, K. Zhang, W. Qian, Y. Huang, D. Huang, Y. Tong, S. Yang, *Angew. Chem., Int. Ed.* **2019**, *58*, 19087.
- [38] Y. Ma, A. Kafizas, S. R. Pendlebury, F. Le Formal, J. R. Durrant, *Adv. Funct. Mater.* **2016**, *26*, 4951.
- [39] B. J. Trzeźniewski, I. A. Digdaya, T. Nagaki, S. Ravishankar, I. Herraiz-Cardona, D. A. Vermaas, A. Longo, S. Gimenez, W. A. Smith, *Energ. Environ. Sci.* **2017**, *10*, 1517.
- [40] C. Cheng, Q. Fang, S. Fernandez-Alberti, R. Long, *J. Phys. Chem. Lett.* **2021**, *12*, 3514.
- [41] X. Shi, I. Herraiz-Cardona, L. Bertoluzzi, P. Lopez-Varo, J. Bisquert, J. H. Park, S. Gimenez, *PCCP* **2016**, *18*, 9255.

- [42] M. Zhou, J. Bao, Y. Xu, J. Zhang, J. Xie, M. Guan, C. Wang, L. Wen, Y. Lei, Y. Xie, *ACS Nano* **2014**, *8*, 7088.
- [43] D. Cardenas-Morcoso, R. Ifraemov, M. García-Tecedor, I. Liberman, S. Gimenez, I. Hod, *J. Mater. Chem. A* **2019**, *7*, 11143.
- [44] F. S. Hegner, I. Herraiz-Cardona, D. Cardenas-Morcoso, N. López, J.-R. Galán-Mascarós, S. Gimenez, *ACS Appl. Mater. Inter.* **2017**, *9*, 37671.
- [45] C. Zachäus, F. F. Abdi, L. M. Peter, R. van de Krol, *Chem. Sci.* **2017**, *8*, 3712.
- [46] R. Irani, P. Plate, C. Höhn, P. Bogdanoff, M. Wollgarten, K. Höflich, R. van de Krol, F. F. Abdi, *J. Mater. Chem. A* **2020**, *8*, 5508.
- [47] E. Y. Liu, J. E. Thorne, Y. He, D. Wang, *ACS Appl. Mater. Inter.* **2017**, *9*, 22083.
- [48] M. Antuch, P. Millet, A. Iwase, A. Kudo, *Appl. Catal., B* **2018**, *237*, 401.
- [49] D. Cardenas-Morcoso, A. Bou, S. Ravishankar, M. García-Tecedor, S. Gimenez, J. Bisquert, *ACS Energy Lett.* **2020**, *5*, 187.
- [50] Z. Tian, P. Zhang, P. Qin, D. Sun, S. Zhang, X. Guo, W. Zhao, D. Zhao, F. Huang, *Adv. Eng. Mater.* **2019**, *9*, 1901287.
- [51] Y. Zhang, X. Chen, F. Jiang, Y. Bu, J.-P. Ao, *ACS Sustainable Chem. Eng.* **2020**, *8*, 9184.
- [52] M. Kan, D. Xue, A. Jia, X. Qian, D. Yue, J. Jia, Y. Zhao, *Appl. Catal., B* **2018**, *225*, 504.
- [53] A. Bou, A. Pockett, D. Raptis, T. Watson, M. J. Carnie, J. Bisquert, *J. Phys. Chem. Lett.* **2020**, *11*, 8654.
- [54] J. Bisquert, G. Garcia-Belmonte, F. Fabregat-Santiago, P. R. Bueno, *J. Electroanal. Chem.* **1999**, *475*, 152.
- [55] J. Bisquert, G. Garcia-Belmonte, F. Fabregat-Santiago, A. Compte, *Electrochem. Commun.* **1999**, *1*, 429.
- [56] S. Ravishankar, C. Aranda, P. P. Boix, J. A. Anta, J. Bisquert, G. Garcia-Belmonte, *J. Phys. Chem. Lett.* **2018**, *9*, 3099.
- [57] L. Bertoluzzi, S. Ma, *PCCP* **2013**, *15*, 4283.
- [58] Y. Liang, T. Tsubota, L. P. A. Mooij, R. van de Krol, *J. Phys. Chem. C* **2011**, *115*, 17594.
- [59] J. A. Seabold, K. Zhu, N. R. Neale, *PCCP* **2014**, *16*, 1121.
- [60] F. F. Abdi, T. J. Savenije, M. M. May, B. Dam, R. van de Krol, *J. Phys. Chem. Lett.* **2013**, *4*, 2752.
- [61] N. Österbacka, F. Ambrosio, J. Wiktor, *J. Phys. Chem. C* **2022**, *126*, 2960.
- [62] W. Wang, P. J. Strohbeen, D. Lee, C. Zhou, J. K. Kawasaki, K.-S. Choi, M. Liu, G. Gallì, *Chem. Mater.* **2020**, *32*, 2899.
- [63] R. Fernández-Climent, S. Giménez, M. García-Tecedor, *Sustainable Energy Fuels* **2020**, *4*, 5916.
- [64] Q. Shi, S. Murcia-López, P. Tang, C. Flox, J. R. Morante, Z. Bian, H. Wang, T. Andreu, *ACS Catal.* **2018**, *8*, 3331.
- [65] F. Tang, W. Cheng, H. Su, X. Zhao, Q. Liu, *ACS Appl. Mater. Inter.* **2018**, *10*, 6228.
- [66] S. Selim, E. Pastor, M. García-Tecedor, M. R. Morris, L. Francàs, M. Sachs, B. Moss, S. Corby, C. A. Mesa, S. Gimenez, A. Kafizas, A. A. Bakulin, J. R. Durrant, *J. Am. Chem. Soc.* **2019**, *141*, 18791.
- [67] D. K. Zhong, S. Choi, D. R. Gamelin, *J. Am. Chem. Soc.* **2011**, *133*, 18370.
- [68] D. Kang, Y. Park, J. C. Hill, K.-S. Choi, *J. Phys. Chem. Lett.* **2014**, *5*, 2994.
- [69] M. N. Shaddad, M. A. Ghanem, A. M. Al-Mayouf, S. Gimenez, J. Bisquert, I. Herraiz-Cardona, *ChemSusChem* **2016**, *9*, 2779.